RSC Advances

PAPER

View Article Online
View Journal | View Issue

Cite this: *RSC Adv.*, 2016, **6**, 68150

Preparation of THPC-generated silver, platinum, and palladium nanoparticles and their use in the synthesis of Ag, Pt, Pd, and Pt/Ag nanoshells†

William W. Bryan,[a] Andrew C. Jamison,[a] Pawilai Chinwangso,[a] Supparesk Rittikulsittichai,[a] Tai-Chou Lee[b] and T. Randall Lee*[a]

Received 26th April 2016
Accepted 14th July 2016

DOI: 10.1039/c6ra10717f

www.rsc.org/advances

Seed nanoparticles of silver, platinum, and palladium (typically ≤4 nm in diameter) were prepared using tetrakis(hydroxymethyl)phosphonium chloride (THPC) as the reducing agent and utilized to generate pure silver, platinum, and palladium nanoshells, along with hybrid platinum/silver nanoshells, on silica cores. The sizes, size distributions, morphologies, chemical compositions, and optical properties of the THPC-metal nanoparticles (THPC-mNPs) were characterized by transmission electron microscopy (TEM), selected area electron diffraction (SAED) analysis, X-ray photoelectron spectroscopy (XPS), Fourier transform-infrared (FT-IR) spectroscopy, and ultraviolet-visible (UV-vis) spectroscopy. Characterization of the resulting nanoshells was performed using scanning electron microscopy (SEM), TEM, and UV-vis spectroscopy. While the use of THPC-gold nanoparticles to seed metal nanoshells is well known, the process is time consuming and requires highly concentrated seeding solutions. Our THPC-mNPs were used to seed the growth of a variety of metal nanoshells in rapid fashion, including the successful generation of highly uniform platinum and palladium nanoshells grown from their own seeds. Efforts to optimize our nanoshell syntheses produced expedited procedures for generating metallic shells with continuous, smooth surfaces.

Introduction

There remains a continued interest in the fabrication of nanomaterials having well-defined and easily modifiable structures. Currently, a variety of types of metal nanoparticles (mNPs) have been pursued that constitute integral components in a number of nanotechnology applications, including nanorods, nanoshells, nanodots, nanocages, nanocubes, nanoflowers, nanostars, and nanodisks.[1–8] Small mNPs composed of platinum, silver, gold, or palladium offer important advantages over other materials due to their ease of fabrication and to their resistance to degradative processes when prepared for specific applications.[9–12] Such mNPs are also desirable because of their unique optical and catalytic properties.[13–17] Extensive nanoparticle research has focused on one of these properties in particular: their surface plasmons, or the coherent oscillation of conducting electrons at the surface of a metal that can be coupled to specific wavelengths of light.[18–20] The most intriguing optical characteristics of metal nanostructures arise from the resulting surface plasmon resonance (SPR), the interaction of photons with these surface electrons when they are in resonance with the frequency of the light. Furthermore, nanomaterials fabricated using noble metals have received considerable interest due to the tunability of these optical properties through the manipulation of their shape and form, producing SPR in the ultraviolet to the near infrared (NIR) regions of the electromagnetic spectrum.[19–23]

Recently, targeted exploitation of these plasmonic properties for medicinal and therapeutic applications has been realized through the assembly of nanoshells.[24] The most widely reproduced nanoshells are core/shell structures composed of dielectric spherical cores (silica) coated with thin metal shells (*e.g.*, gold).[19,25] The surface plasmon properties of such gold nanoshells can be modulated by varying the core size and shell thickness, thus allowing absorption and/or scattering of light over a broad range of visible and NIR frequencies, which contrasts with the narrow range of visible light absorption obtained by a monodisperse sample of simple gold spheres.[26] Moreover, the structure and composition of this type of metal nanostructure can be controllably modified to dictate other physical properties (*e.g.*, magnetic, mechanical, thermal, electro-optical, and catalytic).[27–31] Therefore, metal nanoshells have also been examined for applications involving optical communications, laser-tissue welding, medical imaging, polymer oxidation inhibition, Raman enhancement, and photothermal destruction of pathogens.[32–37]

[a]*Department of Chemistry and the Texas Center for Superconductivity, University of Houston, 4800 Calhoun Road, Houston, TX 77204-5003, USA. E-mail: trlee@uh.edu*

[b]*Department of Chemical and Materials Engineering, National Central University, 300 Jhongda Road, Jhongli City 32001, Taiwan*

† Electronic supplementary information (ESI) available: Contains selected area electron diffraction patterns and Fourier transform infrared spectra of the THPC-generated nanoparticles. See DOI: 10.1039/c6ra10717f

These types of applications have predominantly involved the use of gold or gold alloy nanoshells synthesized by a seed-mediated growth method, with *gold* seeds acting as nucleation sites to grow complete metal shells around a silica core template, even when the targeted nanoshell is another metal. For nanoshell growth utilizing this approach, amines and thiols are typically used as functional groups to attach noble metal nanoparticles to the surface of the core due to their high affinity toward noble metals. Based on prior reports, as well as our own experience, we chose to use 3-aminopropyltrimethoxysilane (APTMS) to functionalize our silica cores due to its repeated success in attaching THPC-gold nanoparticles to various surfaces, as well as to the high zeta potential for the resulting amino-terminated nanoparticles.[38–41] This method achieved preeminence over other synthetic procedures primarily due to its reliability and adaptability; however, the gold seeding process requires an extended exposure of the chemically-modified silica cores to a concentrated seeding solution. Other researchers have approached shell formation *via* the reduction of metal ion precursors onto polymer spheres, oil/water nanodroplets, and tin porphyrin-modified templates, but have not demonstrated the same level of success at growing smooth and continuous metal shells as that obtained using the small mNP seeding method.[42–44]

For our investigation of alternative routes to the successful seeding of metal nanoshells, we started with the preparation of small (typically $\leq$4 nm) silver, platinum, and palladium mNPs using tetrakis(hydroxymethyl)phosphonium chloride (THPC) as both the reducing agent and stabilizing ligand.[45,46] This synthetic route avoids the use of large organic stabilizing molecules that might disrupt the seeding process of the resulting small nanoparticles on the amino-functionalized silica surface. One other important feature is that THPC has been shown to produce small gold nanoparticles reliably with controllable sizes, which are needed for generating smooth nanoshells.[45] We employed transmission electron microscopy (TEM), selected area electron diffraction (SAED) analysis, X-ray photoelectron spectroscopy (XPS), Fourier transform-infrared (FT-IR) spectroscopy, and ultraviolet-visible (UV-vis) spectroscopy to characterize the size, morphology, chemical composition, and optical properties of these THPC-mNP seeds. We then pursued the preparation of metal nanoshells from these seeds forming homogeneous shells of silver, platinum, and palladium. For the latter two monometallic nanoshells, this report provides the first example of their synthesis *via* the THPC-mNP seeded-growth route, and our results compare favorably with those found in the few alternative strategies reported in the literature.[40,47,48] Additionally, we examined how the platinum seeds, which afforded densely populated seeding on silica cores, could be used in a cross-seeding experiment to produce superior silver nanoshells in a significantly shorter time frame than that achieved with gold seeds. All of the nanoshells presented in this report were characterized by scanning electron microscopy (SEM), TEM, and UV-vis spectroscopy. The newly synthesized metal nanoshells and the methods presented herein not only illustrate new and efficient routes to the growth of metal nanoshells with tunable extinction properties, but also offer clarity regarding the fundamental mechanisms of nanoshell growth.

Experimental

Materials

All chemicals were purchased from the indicated suppliers and used as received without additional purification: sodium hydroxide, nitric acid, and hydrochloric acid (EM Science); tetrakis(hydroxymethyl)phosphonium chloride (THPC, 80% in water), formaldehyde, ammonium hydroxide (NH_4OH; 30% NH_3 in water), tetraethylorthosilicate (TEOS), potassium carbonate, 3-aminopropyltrimethoxysilane (APTMS), and silver nitrate ($AgNO_3$; Aldrich); palladium chloride ($PdCl_2$), sodium tetrachloro-palladate(II) (Na_2PdCl_4), and potassium tetrachloroplatinate(II) (K_2PtCl_4; Strem); ethanol (EtOH; Pharmco-Aaper); potassium hydroxide (KOH), and isopropanol (Mallinckrodt Baker). Water was purified to a resistivity of 18 MΩ cm (Academic Milli-Q Water System; Millipore Corporation) and filtered using a 0.22 μm membrane filter. Glassware used for experiments was cleaned in a saturated KOH-isopropanol bath prior to use.

Preparation of THPC silver, platinum, and palladium nanoparticles

Colloidal solutions of small THPC-mNPs were prepared using methods previously reported.[25,45,46,49] For the silver nanoparticles prepared in a THPC solution (THPC-AgNPs), an aqueous solution of sodium hydroxide (0.5 mL, 0.024 g, 0.6 mmol), THPC (12 μL of 80% THPC in 1 mL of water), and 45 mL of Milli-Q water were added to a 100 mL round-bottomed flask and vigorously stirred for 5 min. An aliquot (2 mL, 0.01 g, 0.06 mmol) of aqueous $AgNO_3$ was then added quickly to the mixture. The color of the solution immediately changed from colorless to dark brown-yellow. Vigorous stirring was continued for 10 min. Separately, the palladium nanoparticles generated in a THPC solution (THPC-PdNPs) were prepared in analogous fashion, affording a brown solution. For the procedure, a solution of sodium hydroxide (0.5 mL, 0.02 g, 0.5 mmol), and 1 mL of a THPC solution (12 μL of THPC in 1 mL of water), were vigorously stirred for 5 min in a 100 mL round-bottomed flask containing 45 mL of Milli-Q water. After the allotted time, Na_2PdCl_4 solution (3 mL, 0.02 g, 0.06 mmol) was quickly added to the mixture and stirred for 10 min. Platinum nanoparticles produced from a THPC solution (THPC-PtNPs) were prepared using a slightly different procedure that involved heating 45 mL of water to 90 °C in a round-bottomed flask, and then adding a sodium hydroxide solution (0.5 mL, 0.024 g, 0.6 mmol), and subsequently THPC (12 μL of 80% THPC in 1 mL of water). The solution was vigorously stirred for 1 min, and then 3.0 mL of K_2PtCl_4 was added quickly. The solution was vigorously stirred for 10 min and then cooled to room temperature. During the first 10 min of the cool down, the solution turned dark brown in color. Each of the THPC-mNP seed solutions were used as described in the next paragraph.

Preparation of amine-functionalized silica nanoparticles

Large silica core particles were prepared using a well-known procedure recognized as the Stöber method.[50] Briefly, NH_4OH

(1.0 mL) was added to a mixture of aqueous ethanol (7.0 mL H_2O/12.0 mL EtOH) and stirred at 23 °C for 10 min. Next, TEOS (0.4 mL) was quickly added to the mixture and stirred 5 h, yielding monodisperse silica nanoparticles. For amine functionalization, APTMS (0.5 mL) was then added to the stirred silica-particle solution. Vigorous stirring of the solution was continued overnight for 12 h and then the solution was refluxed 1 h to ensure complete amine functionalization.[51,52] APTMS-coated silica particles were also synthesized in a prior report by our group, which includes complete characterization data for the functionalized core particles.[2,37] To purify the silica particles, the solution was cooled to room temperature, centrifuged (Sorvall Instruments RC-3B refrigerated centrifuge) at 3000 rpm for 1 h and redispersed in 50 mL of ethanol. The cleansing cycle was repeated two times to ensure the purity of the APTMS-functionalized silica nanoparticles. Separately, the attachment of THPC-mNP seeds was accomplished using methods described previously.[38] Briefly, THPC-mNP seeds were assembled onto the silica cores by mixing 45 mL of the THPC-mNP seeds with the amine-functionalized silica cores (0.25 mL) with gentle shaking. The final mixed solutions were allowed to set 4 h, 2 h, and 1 h for the attachment of the THPC-AgNPs, THPC-PtNPs, and THPC-PdNPs seeds, respectively.[38]

Growth of metal nanoshells

For producing the metal nanoshells, the appropriate reducible metal salt solution was first prepared. For silver nanoshells, the growth solution was produced by adding silver nitrate (0.002 g) to 50 mL of water. For platinum nanoshells, this was accomplished by adding 0.5 mL of 1 wt% K_2PtCl_4 to a solution of potassium carbonate (0.008 g in 34 mL of water), followed by vigorous stirring. For palladium nanoshells, a 0.5 mM solution of palladium chloride was prepared by dissolving 0.018 g of $PdCl_2$ in a mixture of 196 mL of water and 4 mL of a 50 mM HCl solution.

The seeded growth of the metal nanoshells was initiated by first stirring 4 mL of the appropriate metal salt solution with varying amounts of THPC-mNP seeded silica nanoparticles (0.1 to 1.0 mL) in a 25 mL beaker for 5 min. It should be noted that adding more silica core particles to a set amount of metal salt solution decreases the shell thickness. Next, the desired metal shell was formed by the reduction of the corresponding metal salt using an appropriate reducing agent. Silver nanoshells were formed by simultaneously adding 50 μL of formaldehyde and 50 μL of ammonium hydroxide. Platinum nanoshells were formed by simply adding 50 μL of formaldehyde, and palladium shells were similarly formed using 0.3 mL of L-ascorbic acid (100 mM). To ensure complete shell growth, the reaction mixtures were vigorously stirred for 5 min. The metal nanoshells were then centrifuged at 2500 rpm for 15 min and redispersed in water, with no signs of aggregation. It is likely that the colloidal stability is afforded by the presence of residual surface formate (for Ag and Pt)[22,37] or ascorbate ions (for Pd).[53]

Characterization methods

All mNPs were characterized by TEM, SAED analysis, XPS, FT-IR spectroscopy, and UV-vis spectroscopy. For the TEM measurements, we used a JEOL JEM-2000 FX electron microscope operating at an accelerating voltage of 200 kV. The samples were deposited from solution onto a holey carbon-coated copper grid and dried at room temperature overnight before analysis by TEM. XPS spectra were collected using a PHI 5700 X-ray photoelectron spectrometer equipped with a monochromatic Al Kα X-ray source ($h\nu = 1486.7$ eV) incident at 90° relative to the axis of a hemispherical energy analyzer. The spectrometer was operated in high-resolution mode with a pass energy of 23.5 eV, a photoelectron takeoff angle of 45° from the surface, and a spot diameter of 2.0 mm. The binding energies were referenced by setting the C 1s binding energy to 284.5 eV. FT-IR spectral data were obtained using a Nicolet Nexus 670 FT-IR spectrometer. The mNPs were deposited from aqueous solution directly onto the surface of a silicon wafer and dried under vacuum overnight. Analysis involved scanning each sample 32 times at a spectral resolution of 4 cm^{-1} and correcting the background. To measure the optical properties of the particles, UV-vis spectra were obtained using a Cary 50 Scan UV-visible spectrometer over the wavelength range of 300–800 nm.

To determine the size and morphology of the nanoshells, the samples were examined using a LEO scanning electron microscope operating at 15 kV. Samples were dropped directly from solution onto silicon wafers and dried at room temperature overnight. High-resolution images were obtained directly from the dried samples without the need for further conductive coatings. SAED studies, as well as high-resolution imaging, were performed using the JEOL TEM instrument described in the preceding paragraph. UV-vis spectra were obtained using the Cary 50 Scan UV-visible spectrometer over the wavelength range of 200–1000 nm. Centrifugation and redispersion in Milli-Q water was performed on all samples prior to analysis.

Results and discussion

To produce silver, platinum, and palladium nanoparticles, we based our synthetic approach on the wet-chemical growth method reported by Duff *et al.*[45,46] While the growth processes observed here are consistent with that reported previously for THPC-gold nanoparticles (THPC-AuNPs), the precise details of the growth mechanism remain obscure. Common to all syntheses are substantial changes in both size and morphology of the THPC-mNPs as the initial concentrations of reactants are varied. The data suggest that changes in particle size and morphology can be rationalized using the La Mer growth model,[54] which describes the kinetics of nanoparticle growth – a process that depends on concentration, is accelerated at elevated temperatures, and leads to an increase in the number of developing particles in solution, with further heating being dominated by Ostwald ripening and consequently larger nanoparticles.

Morphologies and size distributions

THPC-AgNPs were prepared and their TEM images and size distributions are shown in Fig. 1. The images reveal spherical

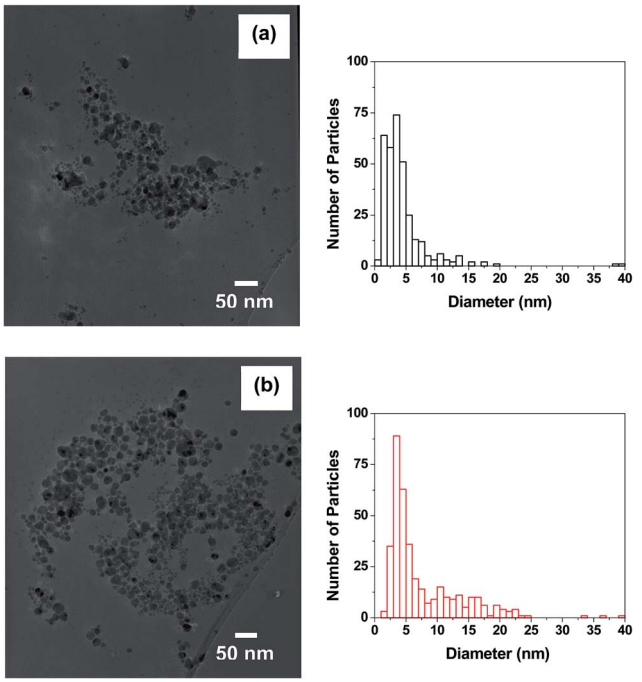

Fig. 1 TEM images of THPC silver nanoparticles and their size distributions obtained using the following silver ion concentrations: (a) 0.6 mM and (b) 1.2 mM.

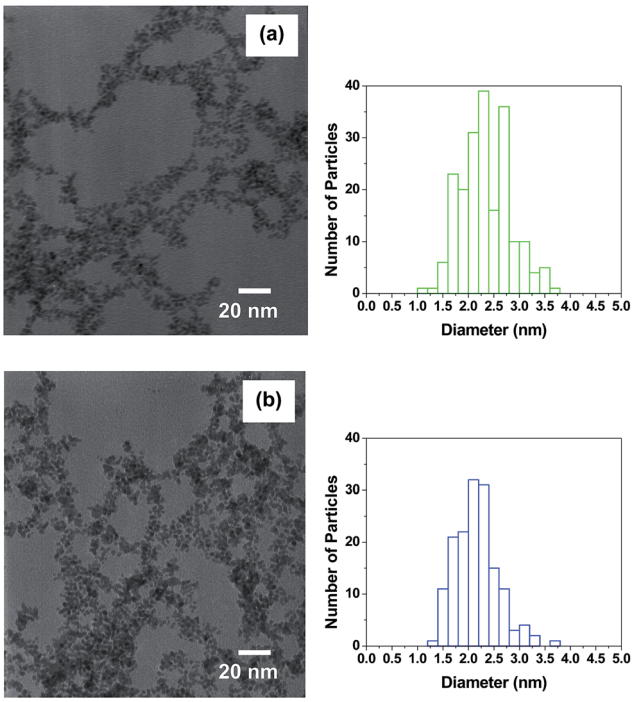

Fig. 2 TEM images of THPC platinum nanoparticles and their size distributions obtained using the following platinum ion concentrations: (a) 0.6 mM and (b) 1.2 mM.

morphologies and relatively high polydispersities. Previous studies of the synthesis of THPC-AuNPs showed increasing sizes with increasing initial concentrations of gold salt.[25] As such, we sought to examine the influence of the concentration of silver salt by using initial silver nitrate concentrations of 0.6 mM and 1.2 mM, and comparing the resultant dimensions and size distributions. At the lower concentration, Fig. 1(a) indicates that an average particle diameter ($\langle d \rangle$) of ~4.4 nm was obtained, and that broad size distributions were present with a coefficient of variation (CV) of 89%.[45] At double the concentration of $AgNO_3$, Fig. 1(b) shows that larger particle sizes are formed ($\langle d \rangle$ = ~7.5 nm) and that a slightly narrower size distribution occurs (CV = 77%); these results are consistent with those reported previously by our group for THPC-AuNPs.[25]

Additional characterization of the silver nanoparticles by selected area electron diffraction reveals the crystalline nature of the particles (see Fig. S1 in the ESI†). The SAED ring pattern suggests that the observed four fringe patterns with spacings of 2.33, 2.04, 1.43, and 1.22 Å are consistent with the fcc polycrystalline silver (111), (200), (220), and (311) lattice planes, with spacings of 2.35, 2.04, 1.44, and 1.23 Å, respectively. Individual spots distributed in the diffraction rings are visible due to the contributions of larger silver nanoparticles.[55]

THPC-PtNPs were also prepared and analyzed by TEM to examine the influence of the reactant concentration. For the synthesis of these nanoparticles, we used heat to facilitate the reaction, which contrasts with our use of ambient temperatures to prepare THPC-AgNPs (*vide supra*) and THPC-PdNPs (*vide infra*). Fig. 2 shows THPC-PtNPs prepared from two different platinum ion concentrations of 0.6 mM Pt and 1.2 mM Pt. The dimensions and size distributions are distinctly smaller and narrower, respectively, when compared to the THPC-AgNPs; furthermore, the platinum nanoparticles appear to be partially aggregated. For the respective platinum ion concentrations, Fig. 2(a) shows that $\langle d \rangle$ = ~2.3 nm and CV = 20%, while Fig. 2(b) shows that $\langle d \rangle$ = ~2.2 nm and CV = 19%. These results suggest that increasing the initial concentration of the platinum ions gives slightly smaller particles. Given, however, the reproducibly small difference and the noted partial aggregation of the THPC-PtNPs, we prefer to draw no strong conclusions here. We also note that prolonged heating times led to complete aggregation of the THPC-PtNPs prepared at both platinum ion concentrations. Examination of the platinum nanoparticles using SAED was also performed (see Fig. S1 in the ESI†), and the data suggest that the observed four fringe patterns with spacings of 2.26, 1.95, 1.38, and 1.19 Å are consistent with the fcc polycrystalline platinum (111), (200), (220), and (311) lattice planes with spacings of 2.25, 1.95, 1.38, and 1.18 Å, respectively.[56]

To prepare THPC-PdNPs, we utilized a procedure analogous to that used to prepare THPC-AgNPs. The TEM images in Fig. 3 illustrate the dimensions and the corresponding size distributions. Concentration effects were also examined at two palladium ion concentrations of 0.6 mM and 1.2 mM. Fig. 3 shows that the particle size decreased with an increase in the initial palladium ion concentration: particles from a 0.6 mM Pd solution produced THPC-PdNPs with $\langle d \rangle$ = ~2.3 nm and CV = 30%, while that from 1.2 mM Pd yielded $\langle d \rangle$ = ~1.7 nm and CV = 37%. The SAED data suggest that the observed patterns are consistent with amorphous palladium (see Fig. S1 in the ESI†).

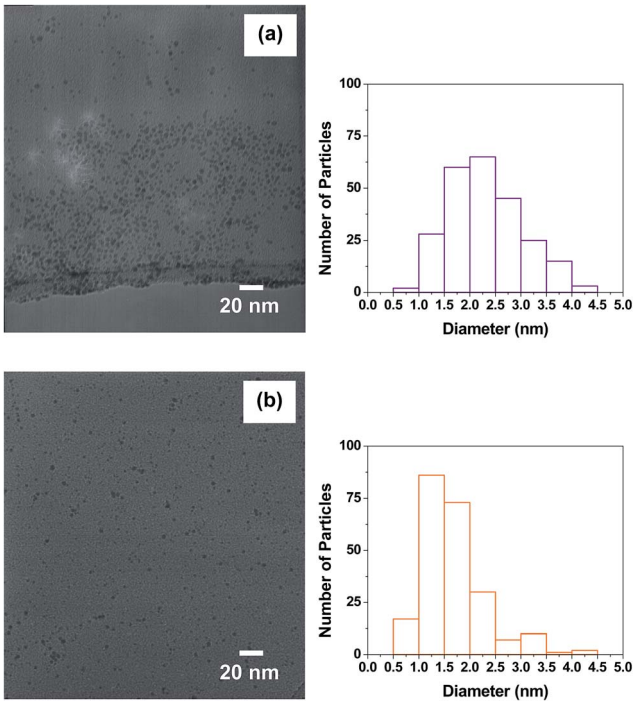

Fig. 3 TEM images of THPC palladium nanoparticles and their size distributions obtained using the following palladium ion concentrations: (a) 0.6 mM and (b) 1.2 mM.

A rationalization for these results might be discerned from a publication by Lu *et al.*, which reported the preparation of small polymer-stabilized palladium nanoparticles.[57] These authors showed that a change in morphology from crystalline to amorphous palladium nanoparticles occured when increasing the rate of reduction using strong reducing agents. Similarly, this study utilized one reducing agent with varying initial concentrations of palladium ions, yielding palladium nanoparticles under our reaction conditions with varying particle sizes yet consistent amorphous structures.

Chemical composition

The elemental composition of the crude and purified THPC-mNPs was evaluated by XPS. For the THPC-AgNPs, Fig. 4(a) and (b) show peaks with binding energies characteristic for Ag $3d_{3/2}$, Ag $3d_{5/2}$, and P $2p_{3/2}$, indicating the existence of silver and phosphorous.[20,58] After centrifugation, decantation, redispersion, and isolation by an additional centrifugation, the P $2p_{3/2}$ peak is markedly diminished, as is evident from Fig. 4(b), which is consistent with the loss of THPC from the sample. Analogous XPS spectra were obtained for the THPC-PtNPs and THPC-PdNPs (Fig. 4(c)–(f)).[20,59–61] Notably, Fig. 4(c) indicates the presence of Pt(II) along with Pt(0); the former can be attributed to incomplete reduction of the platinum salt during synthesis.[20,59,60] For all of the THPC-mNPs, repeated cycles of centrifugation/washing caused the intensity of the P $2p_{3/2}$ peak to decrease relative to that of the metal peak(s) and ultimately disappear (data not shown). As a whole, these data are consistent with a model in which the THPC moieties are loosely bound to the surface of the nanoparticles.

We used FT-IR spectroscopy to evaluate whether the phosphorous in the XPS spectra was derived from THPC. The functional groups of THPC give rise to characteristic bands at 3250, 1600, 1360, and 1000–1100 cm^{-1}, which correspond to O–H stretching, O–H bending, O–H deformation, and C–O stretching vibrations, respectively. As such, the FT-IR spectra in Fig. S2 (see the ESI†) are consistent with the presence of THPC in the unpurified samples. Furthermore, when the nanoparticles were centrifuged and washed, the characteristic peaks for the functional groups of THPC disappeared from the IR spectra (data not shown). Thus, the FT-IR studies confirmed that the phosphorous in the XPS spectra was present as THPC, and that the THPC groups were loosely bound to the surface of the mNPs.

Optical properties

Fig. 5 shows the UV-visible extinction spectra of the silver, platinum, and palladium nanoparticles formed with THPC. The THPC-AgNPs prepared using 0.6 mM and 1.2 mM silver ion concentration exhibited λ_{max} values at ~390 nm and ~392 nm, respectively. These results are consistent with the increase in particle size indicated by TEM (see Fig. 1).[62,63] Notably, the THPC-AgNPs were stable over several weeks with no detectable aggregation. We also collected extinction spectra of the THPC-PtNPs prepared at platinum ion concentrations of 0.6 mM and 1.2 mM. For these samples, the intensity decreased steeply from the ultraviolet region to the visible region. Furthermore, the extinction was more intense for the nanoparticles obtained from the 0.6 mM solution than those obtained using the 1.2 mM concentration. This phenomenon can be attributed to increased particle aggregation at the 0.6 mM concentration. TEM measurements and previous studies of platinum sols are consistent with these results, showing increased coalescence for lower platinum concentrations.[64] Notably, the THPC-PtNPs aggregated and precipitated within ~2 weeks. In a final set of experiments, we collected extinction spectra for the THPC-PdNPs prepared at palladium ion concentrations of 0.6 mM and 1.2 mM. The observations and trends in the data mirrored those of the THPC-PtNPs, including increased coalescence for the lower palladium ion concentration. One notable difference was that THPC-PdNPs aggregated more rapidly than THPC-PtNPs (~36 h *vs.* ~2 weeks). As a whole, the results presented here demonstrate the successful preparation and characterization of THPC silver, platinum, and palladium nanoparticles.

THPC-mNP seeded core particle analyses

TEM analysis was performed to demonstrate successful attachment of the THPC-mNPs onto the silica cores. Fig. 6(a) provides an image of the bare silica template particles, with Fig. 6(b)–(d) providing images of the APTMS-modified silica surfaces decorated with either THPC-AgNPs, THPC-PtNPs, or THPC-PdNPs, respectively. Fig. 6(b) reveals low populations of THPC-AgNP seeds on these surfaces as compared to the THPC-PtNP and THPC-PdNP seed populations exhibited in Fig. 6(c) and (d), respectfully. These TEM images also reveal that the THPC-PtNP and THPC-PdNP seeds are uniformly distributed over the modified silica surfaces. Importantly, the TEM images clearly

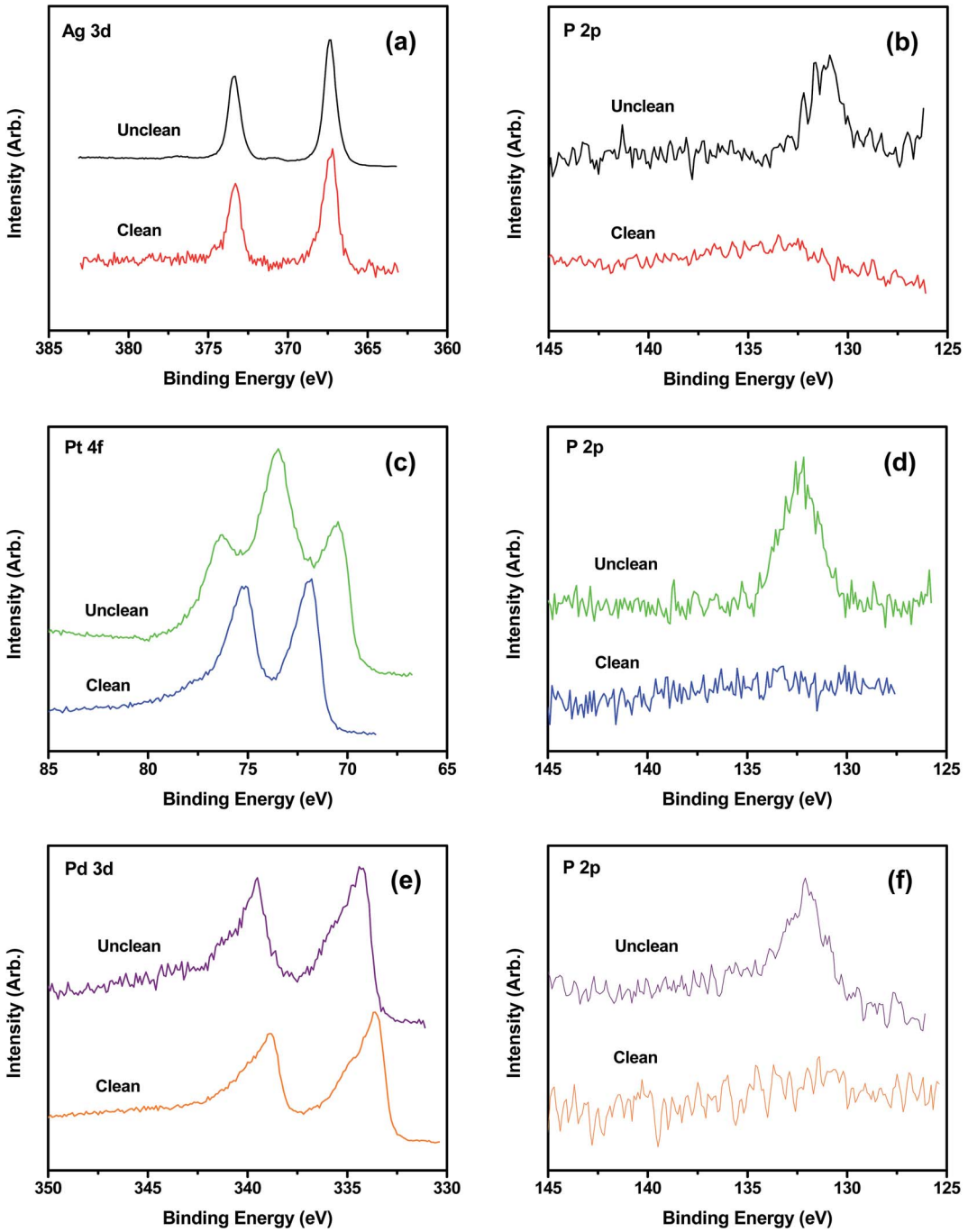

Fig. 4 XPS spectral regions for (a) Ag 3d and (b) P 2p (for silver nanoparticles); (c) Pt 4f and (d) P 2p (for platinum nanoparticles); and (e) Pd 3d and (f) P 2p (for palladium nanoparticles) for the crude ("unclean") and purified ("clean") THPC-mNPs.

demonstrate successful attachment of the THPC-mNPs to the amine-functionalized silica nanoparticle surface. Moreover, the images reveal the manner in which the particles are attached; the particles are both isolated and partially aggregated on the surfaces.

Metal nanoshell analyses

To facilitate the growth of continuous metal nanoshells on the THPC-mNP assemblies, a seeded-growth method was conducted for each metal by means of an appropriately chosen reducing agent. From our experience, as well as in prior reports, formaldehyde and ascorbic acid have demonstrated a propensity to grow smooth metal nanoshells.[2,22,65] Therefore, this initial study focused on the utilization of these reducing agents. Examination of the completed THPC-mNP/metal nanoshells' general size distribution and morphology was accomplished using SEM analysis (Fig. 7), with TEM images revealing greater detail for these composite particles (Fig. 8).

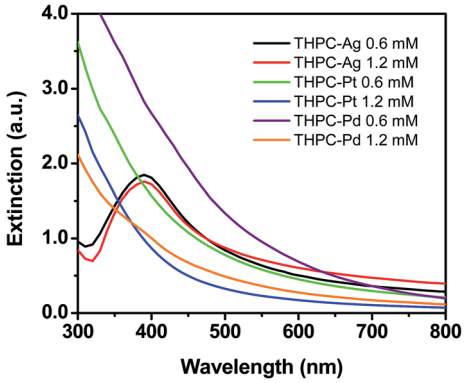

Fig. 5 UV-vis spectra of silver, platinum, and palladium nanoparticles prepared at initial metal ion concentrations of 0.6 mM and 1.2 mM.

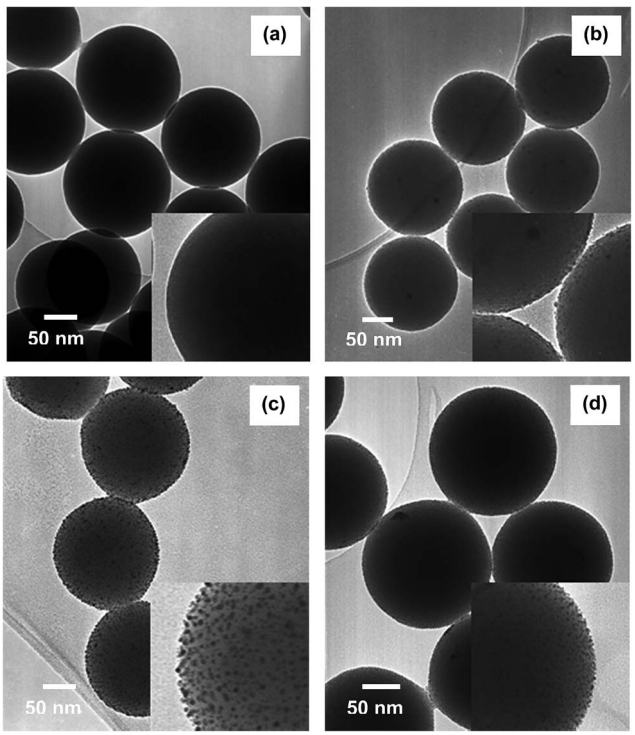

Fig. 6 TEM images of (a) bare APTMS-silica nanoparticles and (b) THPC-AgNPs, (c) THPC-PtNPs, and (d) THPC-PdNPs seeds attached to silica core particles.

Fig. 7(a) provides a typical image for THPC-AgNP/silver nanoshells formed using both formaldehyde and ammonium hydroxide to complete the nanoshell growth. The resulting overall size distribution varies, and the morphological characteristics of the nanoshells reflect the fact that their surfaces are considerably rough. Fig. 8(a) shows in greater detail THPC-AgNP/silver nanoshells that have a total diameter of ~210 nm; this size corresponds to a shell thickness of ~30 nm. The difficulties in controlling the seeded growth of the shell for pure silver nanoshells are revealed in TEM images by a rough inhomogeneous surface coating.[66–68] A possible contribution to the growth of the rough, polydisperse THPC-AgNP/silver nanoshells

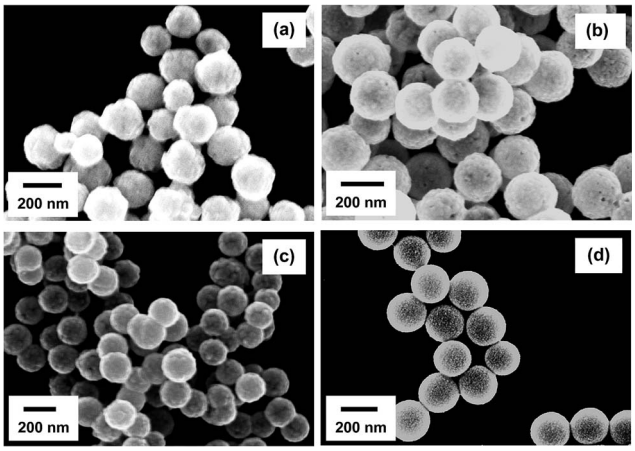

Fig. 7 SEM images of (a) THPC-AgNPs/silver nanoshells, (b) THPC-PtNPs/silver nanoshells, (c) THPC-PtNPs/platinum nanoshells, and (d) THPC-PdNPs/palladium nanoshells. Specific dimensions are provided in the text.

is likely the insufficient presence of nucleation sites (seeds) needed for successful nanoshell growth. A prior report has indicated that it is essential that the metal seeds be densely populated on the surface of the core to produce continuous, smooth shells.[38] For this particular experiment, efforts to improve the silver metal seed density consisted of concentrating the simple THPC-AgNP seeds by evaporation, multiple seeding

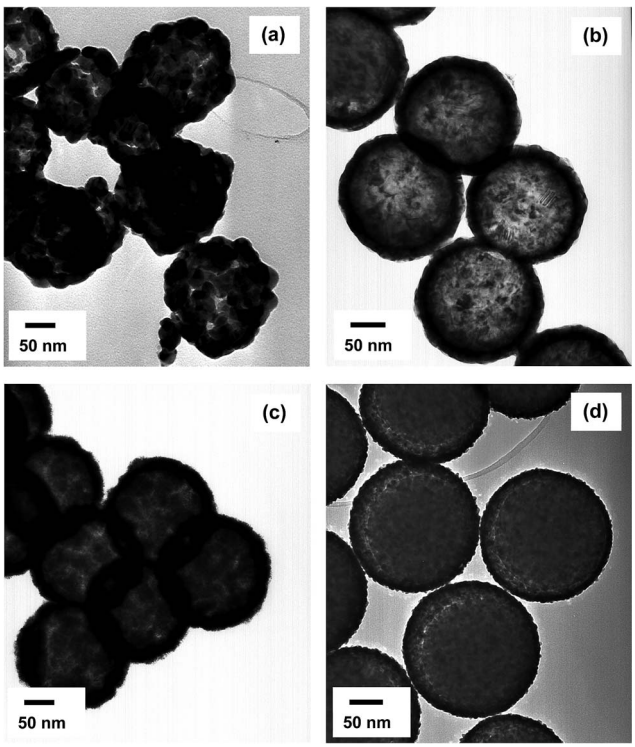

Fig. 8 TEM images of (a) THPC-AgNPs/silver nanoshells, (b) THPC-PtNPs/silver nanoshells, (c) THPC-PtNPs/platinum nanoshells, and (d) THPC-PdNPs/palladium nanoshells. Specific dimensions are provided in the text.

cycles, and centrifugation of the THPC-AgNP solution, along with precipitation of the AgNPs onto silica cores using sodium chloride. All of these efforts proved to be ineffective for accomplishing smooth growth of silver nanoshells from silver seeds. However, utilization of this method consistently produced pure silver nanoshells with improved morphology and dispersity when compared to existing methods. In an effort to improve the morphology of our "silver nanoshells", and narrow the size distribution of the final product, THPC-PtNP-seeded silica spheres were used in a separate experiment to produce a predominantly silver nanoshell. The images for the resulting THPC-PtNP/silver nanoshells (Fig. 7(b) and 8(b)) dramatically contrast with that of the pure silver nanoshells. The TEM image in Fig. 8(b) shows smooth, continuous platinum-seeded silver nanoshells with a diameter of ~200 nm and a shell thickness of ~25 nm.

The growth of pure platinum nanoshells using THPC-PtNP seeds proved to be much more successful than the growth of pure silver nanoshells. Fig. 7(c) shows the general size distribution and morphology of the platinum nanoshells. The TEM image in Fig. 8(c) demonstrates growth of complete THPC-PtNP/platinum nanoshells having diameters of ~200 nm and shell thicknesses of ~25 nm. Unlike THPC-AuNP/gold nanoshells, which require concentrated colloidal THPC-AuNP solutions, the THPC-PtNPs seeds deposited on the silica shells with considerably greater ease using substantially smaller quantities of platinum nanoparticles. Deposition of the platinum seeds occurred within 2 hours, as opposed to deposition of concentrated solutions of gold seeds taking overnight. Much like the deposition of the THPC-PtNPs, full deposition of the THPC-PdNPs required for smooth nanoshell growth was realized in only 1 hour (see Fig. 7(d)). The resulting THPC-PdNP/palladium nanoshells shown in the TEM image in Fig. 8(d) are smooth and continuous and have a diameter of ~190 nm with a shell thickness of ~20 nm.

Optical properties

Fig. 9 displays the UV-vis absorption spectra of the THPC-mNP/metal nanoshells. In general the behavior (*i.e.,* positions, intensities, and broadening) of the absorption bands can be rationalized using Mie theory.[62,69] The slight broadening of the spectra,[6,14,62] likely arises from several factors, such as shell roughness, incomplete shells, and/or overlap of multipole surface plasmon resonances.[70–72] THPC-AgNP/silver nanoshells produce a maximum absorption band at ~550 nm. The shape of the absorption band is clearly different from the absorption band shown for THPC-PtNP/silver nanoshells. The difference consists primarily for regions below 500 nm, which suggest the presence of silver nanospherical aggregates rather than nanoshells.[22] This result is possibly due to the production of discontinuous shells and the presence of distinct silver particle growth at the seeded nucleation sites. The absorption spectrum for THPC-PtNP/silver nanoshells shows behavior much more typical for successful nanoshell growth. Contributions from overlapping multipole surface plasmon resonances are perhaps the most dominant factor due to the large sizes of the nanoshells. Separate experiments (data not shown) show significant optical tunability for the THPC-PtNP/silver nanoshells, but less potential for optical tunability with THPC-AgNP/silver nanoshells due to their inhomogeneous shells. Efforts to enhance the homogeneity of the latter particles are ongoing and will be examined in future reports.

These results are consistent with previous studies of silver nanoshells, which assessed the optical properties of nanospherical aggregates *versus* nanoshells.[22] Also shown in Fig. 9 are the absorption spectra for THPC-PtNP/platinum and THPC-PdNP/palladium nanoshells, which exhibit less pronounced absorption in the visible and infrared regions; however, their morphology is in accord with previous experimental data for AuNP-seeded platinum and palladium nanoshells.[64] Importantly, the UV-vis measurements, along with characterization using TEM and SEM, support a conclusion that we have successfully prepared our targeted metal nanoshells without relying upon AuNP seeds.

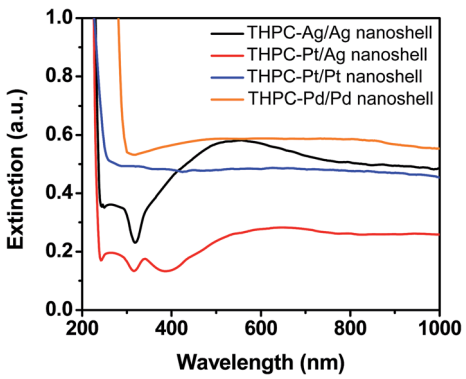

Fig. 9 UV-vis spectra for the THPC-mNP/metal nanoshells.

Conclusions

Small silver, platinum, and palladium nanoparticles with diameters typically ≤4 nm were prepared using simple wet-chemical methods that employed THPC as the reducing agent for nanoparticle seed formation. The dimensions of the THPC-mNPs were varied by adjusting the concentration of the reactants and verified by TEM. SAED data were used to provide further characterization for the three types of seed particles, with the acquired patterns for the THPC-AgNPs and THPC-PtNPs being consistent with fcc polycrystalline particles, while the THPC-PdNPs appeared to be amorphous. Analysis by XPS and FT-IR spectroscopy revealed that the THPC moieties were bound loosely to the surface of the nanoparticles and could be readily removed by centrifugation/washing. The colloidal stability of the THPC-mNPs varied from several weeks (silver) to ~2 weeks (platinum) to ~36 h (palladium).

Synthetic methods were optimized to form metal nanoshells in reliable fashion using the corresponding THPC-mNPs assembled on dielectric silica core particles. We found that using a seeded-growth method facilitates the development of pure metal nanoshells from the corresponding THPC-mNPs without reliance upon conventional methods that use THPC-

AuNPs. However, to improve the morphology and narrow the size distribution of our silver nanoshells, we found it necessary to use the more densely populated THPC-PtNP-seeded silica spheres to produce smooth, uniform metal shells. Characterization of the sizes, size distributions, morphologies, compositions, and optical properties of the metal nanoshells was accomplished by SEM, TEM, SAED, and UV-vis spectroscopy. The facile methods described in this report for synthesizing silver, platinum, and palladium nanoshells should supplement and/or replace existing time-consuming methods that reply upon gold metal seeds.

Acknowledgements

We acknowledge the generous financial support from the Asian Office of Aerospace Research and Development (AFOSR/AOARD FA2386-15-1-4101), the Robert A. Welch Foundation (Grant No. E-1320), and the Texas Center for Superconductivity at the University of Houston. We also thank Dr I. Rusakova for assistance with the TEM measurements.

References

1 J. Becker, I. Zins, A. Jakab, Y. Khalavka, O. Schubert and C. Soennichsen, *Nano Lett.*, 2008, **8**, 1719–1723.
2 J.-H. Kim, W. W. Bryan and T. R. Lee, *Langmuir*, 2008, **24**, 11147–11152.
3 Y.-C. Shiang, C.-C. Huang and H.-T. Chang, *Chem. Commun.*, 2009, 3437–3439.
4 E. C. Cho, C. Kim, F. Zhou, C. M. Cobley, K. H. Song, J. Chen, Z.-Y. Li, L. V. Wang and Y. Xia, *J. Phys. Chem. C*, 2009, **113**, 9023–9028.
5 H. Chen, Z. Sun, W. Ni, K. C. Woo, H.-Q. Lin, L. Sun, C. Yan and J. Wang, *Small*, 2009, **5**, 2111–2119.
6 S. Yi, L. Sun, S. C. Lenaghan, Y. Wang, X. Chong, Z. Zhang and M. Zhang, *RSC Adv.*, 2013, **3**, 10139–10144.
7 A. M. Fales, H. Yuan and T. Vo-Dinh, *J. Phys. Chem. C*, 2014, **118**, 3708–3715.
8 L. Billot, M. Mortier and L. Aigouy, *Plasmonics*, 2013, **8**, 1515–1521.
9 Y. Borodko, L. Jones, H. Lee, H. Frei and G. Somorjai, *Langmuir*, 2009, **25**, 6665–6671.
10 P. D. Nallathamby, K. J. Lee and X.-H. N. Xu, *ACS Nano*, 2008, **2**, 1371–1380.
11 K. Deplanche, R. D. Woods, I. P. Mikheenko, R. E. Sockett and L. E. Macaskie, *Biotechnol. Bioeng.*, 2008, **101**, 873–880.
12 D. Zopes, B. Stein, S. Mathur and C. Graf, *Langmuir*, 2013, **29**, 11217–11226.
13 C.-C. Huang, H.-Y. Liao, Y.-C. Shiang, Z.-H. Lin, Z. Yang and H.-T. Chang, *J. Mater. Chem.*, 2009, **19**, 755–759.
14 J.-F. Li, Y.-F. Huang, S. Duan, R. Pang, D.-Y. Wu, B. Ren, X. Xu and Z.-Q. Tian, *Phys. Chem. Chem. Phys.*, 2010, **12**, 2493–2502.
15 V. Mazumder and S. Sun, *J. Am. Chem. Soc.*, 2009, **131**, 4588–4589.
16 A. Grirrane, A. Corma and H. Garcia, *Science*, 2008, **322**, 1661–1664.
17 J. Han, Y. Liu and R. Guo, *J. Am. Chem. Soc.*, 2009, **131**, 2060–2061.
18 J. Heber, *Nature*, 2009, **461**, 720–722.
19 S. J. Oldenburg, R. D. Averitt, S. L. Westcott and N. J. Halas, *Chem. Phys. Lett.*, 1998, **288**, 243–247.
20 M. R. Jones, K. D. Osberg, R. J. MacFarlane, M. R. Langille and C. A. Mirkin, *Chem. Rev.*, 2011, **111**, 3736–3827.
21 C. Graf and A. van Blaaderen, *Langmuir*, 2002, **18**, 524–534.
22 J. B. Jackson and N. J. Halas, *J. Phys. Chem. B*, 2001, **105**, 2743–2746.
23 P. K. Jain and M. A. El-Sayed, *J. Phys. Chem. C*, 2007, **111**, 17451–17454.
24 Y. Jin, *Acc. Chem. Res.*, 2014, **47**, 138–148.
25 T. Pham, J. B. Jackson, N. J. Halas and T. R. Lee, *Langmuir*, 2002, **18**, 4915–4920.
26 J. Park, J. Joo, S. G. Kwon, Y. Jang and T. Hyeon, *Angew. Chem., Int. Ed.*, 2007, **46**, 4630–4660.
27 H.-L. Liu, J.-H. Wu, J. H. Min, J. H. Lee and Y. K. Kim, *J. Nanosci. Nanotechnol.*, 2009, **9**, 754–758.
28 J.-H. Kim, W. W. Bryan, H.-W. Chung, C. Y. Park, A. J. Jacobson and T. R. Lee, *ACS Appl. Mater. Interfaces*, 2009, **1**, 1063–1069.
29 D. A. Mazurenko, X. Shan, J. C. P. Stiefelhagen, C. M. Graf, A. van Blaaderen and J. I. Dijkhuis, *Phys. Rev. B: Condens. Matter Mater. Phys.*, 2007, **75**, 161102.
30 A. M. Elliott, J. Wang, A. M. Shetty, J. Schwartz, J. D. Hazle and R. J. Stafford, *Proc. SPIE*, 2008, **6865**, 68650Q.
31 K. N. Heck, B. G. Janesko, G. E. Scuseria, N. J. Halas and M. S. Wong, *ACS Catal.*, 2013, **3**, 2430–2435.
32 S. M. Wang, J. J. Xiao and K. W. Yu, *Opt. Commun.*, 2007, **279**, 384–389.
33 A. M. Gobin, D. P. O'Neal, D. M. Watkins, N. J. Halas, R. A. Drezek and J. L. West, *Lasers Surg. Med.*, 2005, **37**, 123–129.
34 G. S. Terentyuk, G. N. Maslyakova, L. V. Suleymanova, N. G. Khlebtsov, B. N. Khlebtsov, G. G. Akchurin, I. L. Maksimova and V. V. Tuchin, *J. Biomed. Opt.*, 2009, **14**, 021016.
35 G. D. Hale, J. B. Jackson, O. E. Shmakova, T. R. Lee and N. J. Halas, *Appl. Phys. Lett.*, 2001, **78**, 1502–1504.
36 M. A. Ochsenkuhn, P. R. T. Jess, H. Stoquert, K. Dholakia and C. J. Campbell, *ACS Nano*, 2009, **3**, 3613–3621.
37 O. Khantamat, C.-H. Li, F. Yu, A. C. Jamison, W.-C. Shih, C. Cai and T. R. Lee, *ACS Appl. Mater. Interfaces*, 2015, **7**, 3981–3993.
38 S. L. Westcott, S. J. Oldenburg, T. R. Lee and N. J. Halas, *Langmuir*, 1998, **14**, 5396–5401.
39 Y. Gao, J. Gu, L. Li, W. Zhao and Y. Li, *Langmuir*, 2016, **32**, 2251–2258.
40 E. Grzincic, R. Teh, R. Wallen, G. McGuire, A. Yella, B. Q. Li and K. Bandyopadhyay, *RSC Adv.*, 2014, **4**, 32283–32292.
41 L.-O. Srisombat, J.-S. Park, S. Zhang and T. R. Lee, *Langmuir*, 2008, **24**, 7750–7754.
42 G. W. Nyce, J. R. Hayes, A. V. Hamza and J. H. Satcher Jr, *Chem. Mater.*, 2007, **19**, 344–346.
43 J. Attia, S. Remita, S. Jonic, E. Lacaze, M. C. Faure, E. Larquet and M. Goldmann, *Langmuir*, 2007, **23**, 9523–9526.

44 H. Wang, Y. Song, Z. Wang, C. J. Medforth, J. E. Miller, L. Evans, P. Li and J. A. Shelnutt, *Chem. Mater.*, 2008, **20**, 7434–7439.
45 D. G. Duff, A. Baiker and P. P. Edwards, *Langmuir*, 1993, **9**, 2301–2309.
46 D. G. Duff, A. Baiker, I. Gameson and P. P. Edwards, *Langmuir*, 1993, **9**, 2310–2317.
47 R. Ashayer, M. Green and S. H. Mannan, *J. Nanopart. Res.*, 2010, **12**, 1489–1494.
48 H. Lee, J.-A. Kwak and D.-J. Jang, *Bull. Korean Chem. Soc.*, 2014, **35**, 945–948.
49 B. K. Teo, K. Keating and Y. H. Kao, *J. Am. Chem. Soc.*, 1987, **109**, 3494–3495.
50 W. Stöber, A. Fink and E. Bohn, *J. Colloid Interface Sci.*, 1968, **26**, 62–69.
51 T. G. Waddell, D. E. Leyden and M. T. DeBello, *J. Am. Chem. Soc.*, 1981, **103**, 5303–5307.
52 A. Van Blaaderen and A. Vrij, *J. Colloid Interface Sci.*, 1993, **156**, 1–18.
53 L. Lu, H. Wang, S. Xia and H. Zhang, *J. Mater. Chem.*, 2002, **12**, 156–158.
54 V. K. LaMer and R. H. Dinegar, *J. Am. Chem. Soc.*, 1950, **72**, 4847–4854.
55 L. Zhang, Y. Shen, A. Xie, S. Li, B. Jin and Q. Zhang, *J. Phys. Chem. B*, 2006, **110**, 6615–6620.
56 Y. Tan, X. Dai, Y. Li and D. Zhu, *J. Mater. Chem.*, 2003, **13**, 1069–1075.
57 W. Lu, B. Wang, K. Wang, X. Wang and J. G. Hou, *Langmuir*, 2003, **19**, 5887–5891.
58 Y. Chen and X. Wang, *Mater. Lett.*, 2008, **62**, 2215–2218.
59 I. Lee, R. Morales, M. A. Albiter and F. Zaera, *Proc. Natl. Acad. Sci. U. S. A.*, 2008, **105**, 15241–15246.
60 M. Zhao and R. M. Crooks, *Adv. Mater.*, 1999, **11**, 217–220.
61 C. Evangelisti, N. Panziera, P. Pertici, G. Vitulli, P. Salvadori, C. Battocchio and G. Polzonetti, *J. Catal.*, 2009, **262**, 287–293.
62 G. Mie, *Ann. Phys.*, 1908, **25**, 377–445.
63 S. Link, Z. L. Wang and M. A. El-Sayed, *J. Phys. Chem. B*, 1999, **103**, 3529–3533.
64 D. G. Duff, P. P. Edwards and B. F. G. Johnson, *J. Phys. Chem.*, 1995, **99**, 15934–15944.
65 J.-H. Kim, H.-W. Chung and T. R. Lee, *Chem. Mater.*, 2006, **18**, 4115–4120.
66 Z.-J. Jiang and C.-Y. Liu, *J. Phys. Chem. B*, 2003, **107**, 12411–12415.
67 K. Wang, X. Zhang, C. Niu and Y. Wang, *ACS Appl. Mater. Interfaces*, 2014, **6**, 1272–1278.
68 C. Tian, E. Wang, Z. Kang, B. Mao, C. Zhang, Y. Lan, C. Wang and Y. Song, *J. Solid State Chem.*, 2006, **179**, 3270–3276.
69 A. L. Aden and M. Kerker, *J. Appl. Phys.*, 1951, **22**, 1242–1246.
70 S. J. Oldenburg, S. L. Westcott, R. D. Averitt and N. J. Halas, *J. Chem. Phys.*, 1999, **111**, 4729–4735.
71 S. J. Oldenburg, G. D. Hale, J. B. Jackson and N. J. Halas, *Appl. Phys. Lett.*, 1999, **75**, 1063–1065.
72 S. J. Oldenburg, J. B. Jackson, S. L. Westcott and N. J. Halas, *Appl. Phys. Lett.*, 1999, **75**, 2897–2899.